The EuroBiotech Journal
RESEARCH ARTICLE
Medicine and Biotechnology

Anatomical characterization of ADHD using an atlas-based analysis: A diffusion tensor imaging study

Niyazi Acer[1], Nazan Dolu[2], Gokmen Zararsiz[3], Mehmet Sait Dogan[4], Kazim Gumus[5], Sevgi Ozmen[6], Ali Yucel Kara[2], Handan Soysal[7], Huseyin Per[8] and Mehmet Bilgen[9]

Abstract

Purpose: To examine brain diffusion characteristics in pediatric patients with attention deficit hyperactivity disorder (ADHD) using diffusion tensor imaging (DTI) and an atlas-based anatomical analysis of the whole brain and to investigate whether these images have unique characteristics that can support functional diagnoses.

Materials and Methods: Seventeen children with ADHD and ten control subjects (all age-matched) underwent MRI scans. The Institutional Ethics Board approved this study. Morphometric analysis was performed using MriStudio software. The diffusion images were normalized using a linear transformation, followed by large deformation diffeomorphic metric mapping (LDDMM). For 189 parcellated brain regions, the volume, fractional anisotropy (FA), mean diffusivity (MD), axial diffusivity (AD), and radial diffusivity (RD) were measured.

Results: Children with ADHD were found to have increase in the body of lateral ventricle volumes compared to the control. Increased MD was found in the deep gray matter, amygdala, thalamus, substantia nigra, and also the cerebellum left and right side. Increased RD was found in the deep gray matter, caudate, thalamus, substantia nigra and hippocampus left and right side compared to the control. Significant elevated FA was found in the bilateral splenium of the corpus callosum in ADHD patients.

Conclusion: Children with ADHD display abnormal diffusion characteristics and anatomical features compared to healthy controls. DTI can provide sensitive information on integrity of white matter (WM) and intra-WM structures in ADHD.

[1]Department of Anatomy, Faculty of Medicine, Erciyes University, Kayseri, Turkey
[2]Department of Physiology, Faculty of Medicine, Erciyes University, Kayseri, Turkey
[3]Departmentof Biostatistics, Faculty of Medicine, Erciyes University, Kayseri, Turkey
[4]Department of Radiology, Faculty of Medicine, Erciyes University, Kayseri, Turkey
[5]Biomedical Imaging Research Center, Erciyes University, Kayseri, Turkey
[6]Department of Child Psychiatry, Faculty of Medicine, Erciyes University, Kayseri, Turkey
[7]Department of Anatomy, Faculty of Medicine, Baskent University, Ankara, Turkey
[8]Department of Pediatrics, Faculty of Medicine, Erciyes University, Kayseri, Turkey
[9]Department of Biophysics, Medical Faculty, Adnan Menderes University, Aydin, Turkey

Corresponding Author: Niyazi Acer
E-mail: acerniyazi@yahoo.com

Published online: 27 January 2017
doi:10.24190/ISSN2564-615X/2017/01.08

Introduction

Attention deficit hyperactivity disorder (ADHD) is a common neuropsychiatric disorder of childhood and persists during adult age, affecting millions of people (1). ADHD prevelance is between 3% and 5% of children and young persons with an overrepresentation of boys by approximately 3:1 ratio (2).

Neuroimaging studies have demonstrated that ADHD results in different morphometrical characteristics in certain brain regions, such as prefrontal and parietal cortex, basal ganglia, and limbic structures (3, 4). In children with ADHD, reduction in total cerebral volume, corpus callosum and cerebellar volume have also been reported (5, 6). Although, the exact mechanism has not yet been clarified, ADHD is presumed to be linked to dysfunction of the frontal–striatal–cerebellar circuits (1, 7), and thus abnormalities in white matter (WM) development has been suggested as an important factor in the its pathophysiology (8).

In recent years, diffusion tensor imaging (DTI) has become the method of choice to investigate WM pathology in neuropsychiatric disorders. DTI is a magnetic resonance imaging (MRI) technique developed for mapping diffusion characteristics within soft biological tissue and thus used extensively to characterize the underlying WM microstructure based on the measurement of restricted diffusion of water molecules (9-11). In previous studies, ADHD in children has been investigated with DTI and variations in tensor-derived indices mean diffusivity (MD), fractional anisotropy (FA), axial diffusivity (AD) and radial diffusivity (RD) have been characterized as summarized in a review pa-

per (11-14). However, the previous reports were either partial or limited as they either focused on specific regions of the brain or examined only one or two of the indices. Therefore, a comprehensive approach was needed to evaluate the whole brain. Thus, the current study was initiated to examine the brains of children with ADHD with quantitative characterization based on an atlas-based analysis (ABA) as applied to the data obtained from anatomical and diffusion tensor imaging modalities. In the following, we provide complete and detailed maps of the changes in volumes and diffusion indices as measured from 189 anatomical subregions of the brains with ADHD as referenced to the control group.

Materials and Methods

Subjects

A group of 17 children with ADHD were recruited along with 10 age-matched healthy controls for comparison. There were no significant age differences between the two groups ($p>0.05$). The Ethics Board at Erciyes University approved the study plan and written informed consents were obtained from the parents of the participants.

All subjects were right-handed. ADHD was diagnosed by two pediatric psychiatrists according to the DSM-IV criteria (American Psychiatric Association, 1994). Wechsler Intelligence Scale for Children-Revised (WISC-R) was 101.3 (SD=12.3, IQ range 75–119) in the ADHD group, and 108.6 (SD=8.2, IQ range 94–131) in the control group. Patients with mental retardation (MR; IQ<75), psychiatric comorbidities and those with known neurological and metabolic disorders were excluded.

The eligibility for control subjects included the following: normal developmental history, attendance at a regular school, no history of seizures or head injury, no clinical evidence of neurological dysfunction and normal imaging as judged by a clinical neuroradiologist (MSD). The control data were obtained from the patients with benign seizures that had no neurological sequelae (n= 8) or headache (n = 2) and who were diagnosed as normal by a pediatric neurologist (HP, SO). Males and females in all groups did not differ significantly by age ($p=0.68$).

Neuroimaging

Neuroimaging was performed at Erciyes University, Radiology Department using a 1.5 T Siemens Aera scanner (Siemens, Germany). Anatomical images were acquired in the sagittal plane using T1-weighted 3D MPRAGE sequence, with parameter setting: TE/TR=2.67 ms/1.9s, flip angle = 81°, acquisition matrix = 256 x 256, FOV=256 mm^2, number of slices = 160 and slice thickness=1.0 mm.

DTI involved spin-echo sequence with single-shot, echo-planar acquisition . Balanced pairs of diffusion gradients were applied along 21 orthogonal directions using b value of 0 and 1000 s/mm^2 with other paramters being set to TR=3500ms, TE=83ms, FOV=230 mm^2, matrix = 128 × 128 and slice thickness = 5 mm. The acquisition time per dataset was approximately 4 minutes.

The original raw data were transferred from the scanner to the DICOM format and anonymized. The DTI datasets were transferred to a personal computer running Windows platform and were further processed offline using MriStudio (www.MriStudio.org) (15).

DTI processing

MRIStudio has become widely used in neuroimaging studies of MRI and DTI data (15-17). MRIStudio consists of three programs: DTIStudio (18), DiffeoMap and ROIEditor (19). DTIStudio is a package for the visualization and processing of diffusion MR data. DiffeoMap is used for image transformation based on a large deformation diffeomorphic metric mapping (LDDMM). ROIEditor is a program that uses the results of DiffeoMap to perform image analysis with respect to a single atlas both at the voxel and regional level (19).

In this study, the raw diffusion-weighted images were registered to the first b0 images using a 12-mode affine transformation of Automated Image Registration (AIR) to minimize misregistrations due to subject motion(16). All individual images were visually inspected to discard those with artifacts. The six elements of the diffusion tensor and the indices FA, MD, RD and AD were all calculated using DTIStudio (20). The masked images of each participant were then used for Large Deformation Diffeomorphic Metric Mapping (LDDMM) (21, 22). After stripping the skull, the images were first normalized linearly to the JHU-DTI-MNI "Eve" template with a nine-parameter affine transformation of AIR. Then, a nonlinear transformation, accomplished by dual-contrast LDDMM, was applied, using b0 and FA images (16).

The three principal diffusivities (eigenvalues, $\lambda1 > \lambda2 > \lambda3$) denote the diffusion coefficients measured along the three principal axes of a diffusion ellipsoid. The spatial orientation of fibers can be derived from the eigenvectors of the diffusion tensor (23). FA describes the deviation of the diffusion ellipsoid from spherical (isotropic diffusion) case (24-26) and is given by

$$FA = \frac{\sqrt{(\lambda_1-\lambda_2)^2+(\lambda_2-\lambda_3)^2+(\lambda_3-\lambda_1)^2}}{\sqrt{2(\lambda_1^2+\lambda_2^2+\lambda_3^2)^2}}$$

Parallel ($\lambda1$) and perpendicular ($\lambda2$ and $\lambda3$) diffusion direction relative to the fiber orientation are referred to, respectively, as axial diffusivity (AD), $\lambda II= \lambda1$ and radial diffusivity (RD), $\lambda1=(\lambda2+ \lambda3)/2$ (27).

Mean diffusivity (MD), $(\lambda1+ \lambda2+ \lambda3)/3$, or trace, $\lambda1 + \lambda2 + \lambda3$) denotes the rate of diffusion averaged over all directions (26). MD is proportional to the volume of the ellipsoid characterized by the diffusion tensor and quantifies the absolute amount of diffusion in a voxel (10, 24, 25, 28, 29).

The masked images of each participant were first transformed linearly using affine AIR transformation, with trilinear interpolation and then non-linearly using LDDMM with cascading alpha of 0.01, 0.005 and 0.002, in order to match with

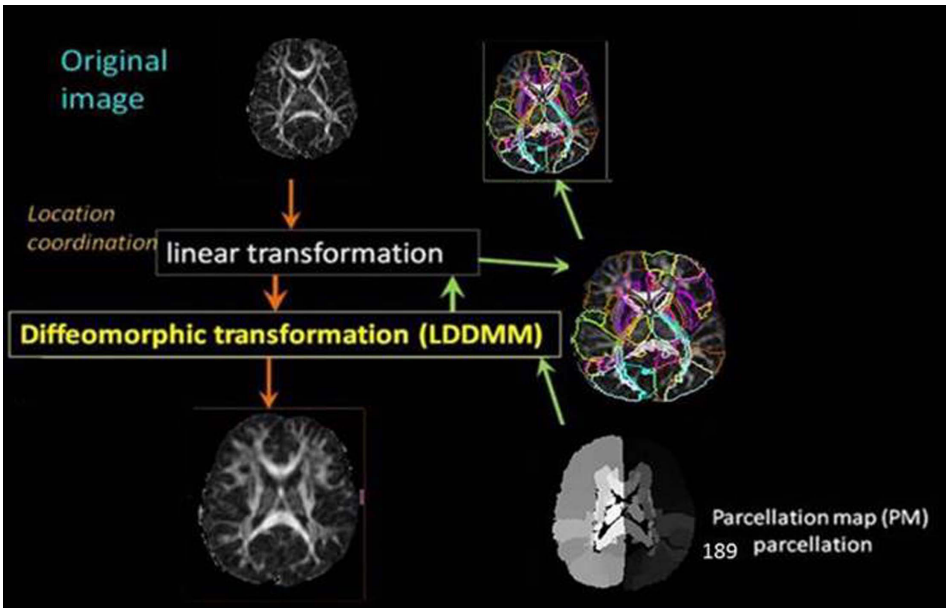

Figure 1. Image normalization process. The orange arrows show forward transformation, the subject's original image was firstly linearly normalized (affine transformation), followed by non-linear normalization (LDDMM). The green arrows show backward transformation, the brain parcellation maap was transformed to the original MR image using the same deformation fields. This allows the map to be superimposed onto the original images with parcellation into 189 structures. This figure is modified using Yoshida et al. (2013) study.

the corresponding Johns Hopkins University MNI-space single participant skull-stripped templates (JHU_MNI_B0 _ss, Trace and FA_ss) (30).

Next, the inverse transformation algorithms using inverse LDDMM and then inverse AIR were applied to the ROI atlas (JHU_MNI_SS_WMPM_TypeII_V2.1), in order to obtain ROIs that are within each participant's original brain space so leading to the parcellation of the brain into 189 anatomical structures (30). These procedures were reciprocal, so that the inverse-transformed brain parcellation map was superimposed onto the original FA, RD and Trace images leading to parcellation of the brain into 189 anatomical structures (17, 22). As a result, the quantitative volume values (number of voxels), FA, MD, AD and RD measured for 189 parcellated brain structures were obtained for each participant (15, 30) (**Fig. 1**).

By using ROIEditor, the FA, MD, AD, RD values and volume of each region was automatically measured after each image was linearly normalized to the ICBM space (22).

A predefined comprehensive white matter atlas was combined with highly non-linear image registration methods for automated 3D white matter segmentation. We applied fully segmented white matter atlases in ICBM-152 and Talairach spaces that contain as many as 189 predefined 3D anatomical regions. Highly non-linear LDDMM was used for normalization (22).

Statistical Analysis

A two-sided t test with independent samples was performed to compare the differences between the ADHD and control groups. p values were adjusted using the Benjamini-Hochberg procedure to control the multiple testing adjustment problem (31). For classification analysis, nearest shrunken centroids algorithm was applied. Feature selection procedure was applied using the lasso method and estimation was conducted using diagonal linear discriminant analysis algorithm (32). The data set was split into training and test datasets as 70% and 30%, respectively (Hastie 2014). Training data sets were used for model building and a test was used for model validation and performance assessment. To optimize the threshold parameter, a five-fold cross-validation method was used. Sensitivity, specificity, positive and negative predictive values and accuracy rates were calculated. All analyses were performed in various packages (pamr, gplots, genefilter) of R 3.2.0 (33) (www.r-project.org).

Results

The ADHD and control groups consist of right handed children with no significant differences in their age and sex (**Table 1**). The volumes in the two groups as measured from the atlas-based analysis in 189 regions are shown in **Table 2**. Overall, most of the regions in children with ADHD were smaller, but not significantly different ($p<0.05$) to the controls, except in

Table 1. Demographic characteristics

		Control n=10	ADHD n=17
Gender	N boys/girls	7/3	15/2
Age	Mean (SD)	10.21(2.1)	10.55 (2.8)
	Range	7-14	7-14
Handedness	Right/left	10/0	17/0

the lateral ventricle volumes in both right and left hemispheres (LV_body_R, LV_body_R). The measurements revealed significantly higher MD values in the ADHD group relative to the controls, bilaterally in MCP, SCP, ICP, PGH, STG, MFG_DFPC, ML, insula, cerebellum, substantia nigra, amiygdala, thalamus, pons and hippocampus (**Fig. 2a,b**).

Significantly increased FA were found in ADHD patients in the UNC, PLIC, SCR, ACR and substantia nigra right, as well as in the bilateral splenium of the corpus callosum. Also, significantly increased FA were found in ADHD patients in the TAP, subgenual ACC, Midbrain, PTR and MTG (**Fig. 3**). Significantly higher RD values in the ADHD group relative to controls, bilaterally in the entorhinal cortex, MCP, caudate, thalamus, hippocampus, substantia nigra and ML. Significantly decreased AD were found bilaterally in the red nucleus in ADHD patients (**Fig. 4**).

Using nearest the shrunken centroids algorithm and Ins, SCP measurements given in the table, permit classification of ADHD disease based on the MD measurement of the left side of the brain with 100% sensitivity and 50% specificity as well

Table 2. Between-group differences in some brain structures for volumes (mm^3)

Variable	ADHD	SD	Control	SD	statistic	dm	p.value
LV_body_L	2694,47	383.84	1926,90	1187,07	1,97	767,57	0,05*
RLIC_L	1748,87	236,53	1935,20	228.44	-1,96	-186,33	0,06
EC_L	3468,27	287,01	3700,10	323.47	-1,88	-231,83	0,07
CST_L	1210,00	187,40	1328,30	165,72	-1,62	-118,30	0,12
PSMG_L	17916,6	1945,66	19352,20	2590,66	-1,58	-1435,53	0,13
MOG_L	34497,5	5562,10	38383,90	6682,78	-1,58	-3886,37	0,13
Snigra_L	129,40	28,39	145,30	22,31	-1,57	-15,90	0,13
PCT_L	696,87	113,64	777,60	150,39	-1,53	-80,73	0,14
LV_frontal_L	3043,60	1087,93	2500,70	376,14	1,51	542,90	0,14
PCR_L	2414,87	291,30	2258,20	212,21	1,46	156,67	0,16
SCC_L	5105,67	768,23	4709,70	514,08	1,43	395,97	0,17
Medulla_L	1401,80	160,13	1491,40	158,43	-1,38	-89,60	0,18
GP_L	1138,33	132,05	1223,30	1792,12	-1,37	-84,97	0,18
AnteriorCom_L	85,13	17.14	92,40	13,17	-1,28	-7,27	0,21
ICP_L	761,80	120.95	811,90	121.39	-1,28	-50,10	0,21
LFOG_L	7752,53	1171,35	8619,00	1916,19	-1,27	-866,47	0,22
PLIC_L	2591,73	342,83	2792,80	342,83	-1,25	-201,07	0,22
CGH_L	1258,13	134,32	1331,20	171,32	-1,19	-73,07	0,24
PSTG_R	7823,53	885,86	9574,60	885,86	-4,96	-1751,07	0,00*
LV_body_R	2595,33	913,83	1970,30	426,13	2,01	625,03	0,04*
LV_frontal_R	3189,00	902,00	2657,80	404,85	1,74	531,20	0,10
ML_R	670,93	76,83	723,00	78,17	-1,65	-52,07	0,11
LenticularFasc_R	232,47	22,89	251,60	22,89	-1,65	-19,13	0,11
CST_R	1147,33	146,67	1250,80	180,65	-1,58	-103,47	0,13
SCP_R	1164,93	110,79	1228,50	84.67	-1,54	-63,57	0,14
MTG_R	11731,2	1706,55	12706,70	1377,70	-1,51	-975,43	0,15
RLIC_R	1750,33	191,78	1858,20	169,22	-1,44	-107,87	0,16
LV_atrium_R	1402,73	505,14	1158,30	295,73	1,38	244,43	0,18
PSIG_R	10459,5	1452,34	11247,30	1341,14	-1,37	-787,77	0,18
PCT_R	876,60	126,95	956,40	168,21	-1,35	-79,80	0,19
AG_R	29670,9	3654,48	31899,10	4316,96	-1,34	-2228,17	0,19
MFG_DPFC_R	21847,0	4136,57	23863,50	2816,63	-1,34	-2016,43	0,19
SCC_R	5607,80	712,31	5237,90	669,78	1,30	369,90	0,21
PSMG_R	13894,2	2099,34	14879,20	1561,92	-1,26	-984,93	0,22
CP_R	1432,20	166,42	1524,40	199,34	-1,25	-92,20	0,22
Hippo_R	4093,07	542,61	3863,80	251,76	1,24	229,27	0,23

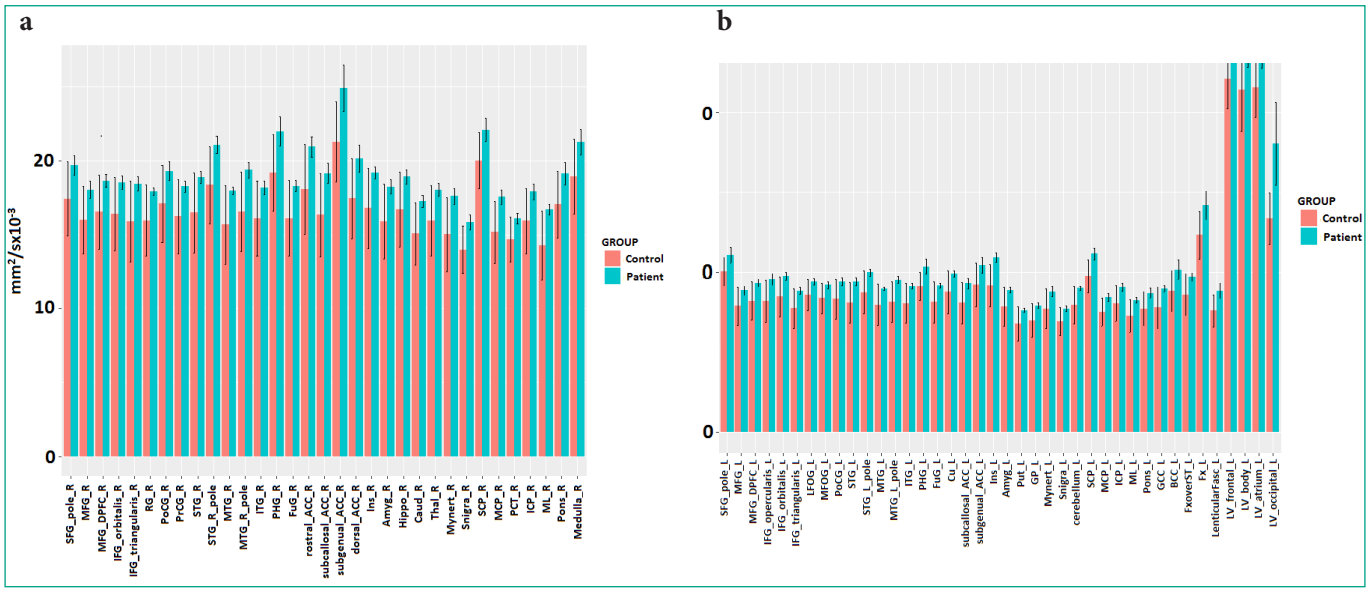

Figure 2a,b. MD values ($mm^2/s \times 10^{-3}$).

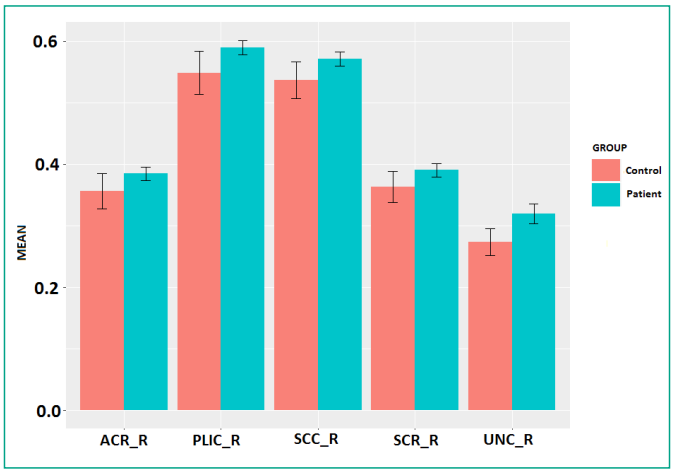

Figure 3. FA values.

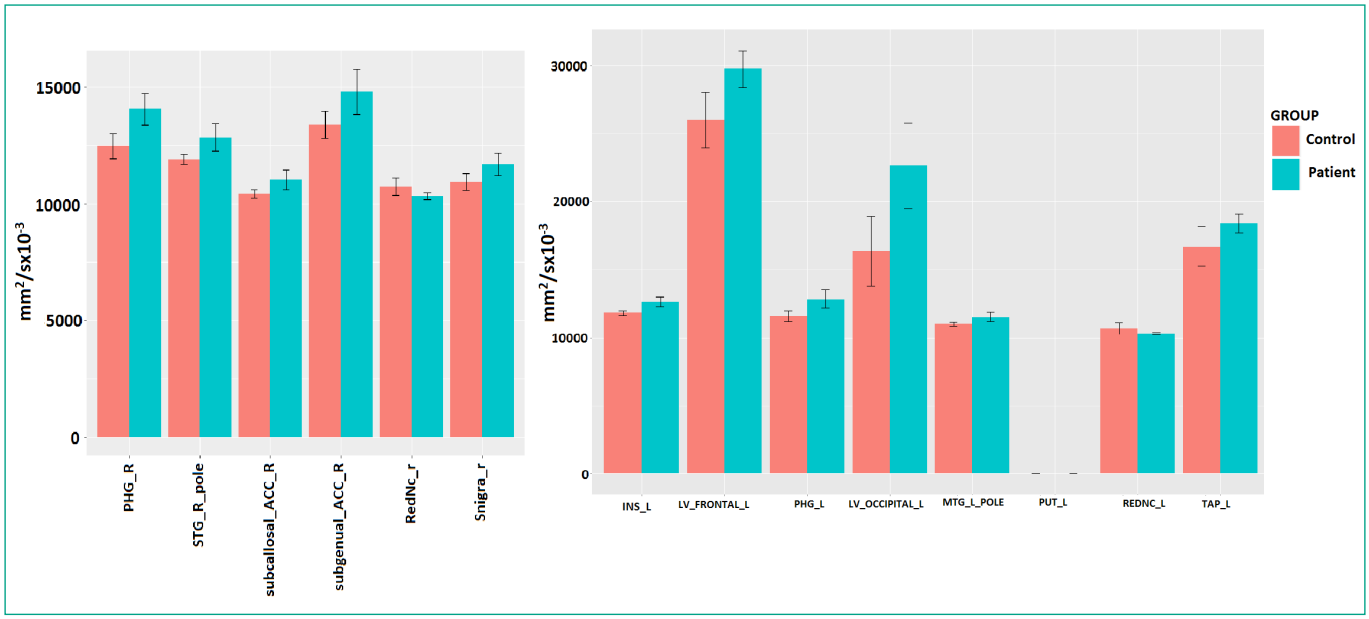

Figure 4. AD values ($mm^2/s \times 10^{-3}$).

Table3. Statistical measurments displaying the neasrest shrunken centroids classification results

Left						
Measure	**Features**	**SEN(%)**	**SPE(%)**	**PPV(%)**	**NPV(%)**	**ACC(%)**
FA	*TAP, PTR, FX/ST, Subgenual_ACC, MTG, Midbrain, CP, PLIC, Lenticular_Fasc*	100.00	0.00	66.67	0.00	66.67
AD	*Ins, LV_frontal, RLIC, ACR, LV_occipital, LV_atrium, Put, OlfactoryRadiation, Thal, LV_body, SFG, Tap, RedNC, PHG*	83.33	50.00	83.33	50.00	75.00
MD	*Ins, LV_frontal, SCP*	100.00	50.00	71.43	100.00	77.78
RD	*MCP*	71.43	50.00	83.33	33.33	66.67
Volume	*PCR, Snigra, AnsaLenticularis*	100.00	0.00	62.50	0.00	62.50
Right						
Measure	**Features**	**SEN(%)**	**SPE(%)**	**PPV(%)**	**NPV(%)**	**ACC(%)**
FA	*SFO, UNC*	100.00	0.00	66.67	0.00	66.67
AD	*PHG, ML, STG_pole, RedNC, Snigra, Subcallosal_ACC, LV_frontal, FX, MTG_pole, ENT, Mynert, IFG_triangularis, SFO, Subgenual_ACC, Amyg, PCT, SFG_pole, STG, RG, Hippo, OlfactoryRadiation, SLF, Fug, rostral_ACC*	66.67	100.00	100.00	50.00	75.00
TMD	*Snigra, Pons, MCP, Caud, Mynert, ML, Subcallosal_ACC, MTG_Pole, Thal*	100.00	0.00	88.89	0.00	88.89
RD	*Caud, Ent, ML*	100.00	0.00	33.33	0.00	33.33
Volume	*PSTG*	100.00	0.00	50.00	0.00	

as Ins, LV_frontal, RLIC, ACR, LV_occipital, LV_atrium, Put, Olfactory radiation, Thal, LV_body, SFG, Tap, RedNC, PHG based on AD measurements of the left side of the brain with 83.33% sensivity and 50% specificity. Other classification results and the selected subset of features for each measurement are given in **Table 3**.

Discussion

We found that chidren with ADHD had a significantly larger body of lateral ventricle volume compared to the controls. Most brain regions were smaller in children with ADHD, but they were no significant differences between ADHD and controls. Atlas-based analysis revealed significantly higher MD, FA, RD and AD values in the ADHD group relative to the controls concerning the cerebellum, substantia nigra, amiygdala, pons, caudate, thalamus, hippocampus, red nucleus, splenium of corpus callosum.

Structural imaging studies have reported the abnormal development of some brain regions in ADHD such as the prefrontal cortex, cerebellum, striatum and basal ganglia, corpus callosum and the parietal cortex (6, 34, 35-37). Anatomical studies indicate widespread decreases in volume throughout the cerebrum and cerebellum as well as the prefrontal cortex, the basal ganglia, the dorsal anterior cingulate cortex and the corpus callosum. The most replicated alterations in ADHD in childhood include significantly smaller volumes in the prefrontal cortex (PFC), caudate, splenium of the corpus callosum, cerebellum and overall cerebral volume (38).

Volumetric studies of the some brain areas in children with ADHD have generated conflicting results. Some authors suggested that the caudate nuclei of children with ADHD are larger (39, 40) while some are smaller than the controls (2, 38, 41).

Previous studies have shown smaller brain volume and less gray matter in children with ADHD (42).

More recently, advanced imaging techniques have found basal ganglia and frontal region structure abnormalities in ADHD. Some studies indicate that the frontal lobe is an important place for research on ADHD for a number of reasons (5, 42). Lopez-Larson et al. (2012) found reductions in the bilateral insular gray matter volumes in youths with ADHD compared to the controls (37).

There are two main analytical methods that can be employed in the investigation of DTI measurements: voxel-based analysis (VBA) and region-of-interest analysis (ROI). VBA allows for whole-brain analysis, thus providing a complete overview of white matter integrity in the brain. Many studies investigating specific ROIs have been published. Comparability among ROI studies can be limited since the choice and placement of ROIs are subjective (11, 43). In a recent study, eleven ROIs were chosen based on their possible relevance to functional deficits in ADHD: the body, splenium and genu of the corpus callosum, anterior and posterior corona radiata, anterior and posterior limbs of the internal capsule, superior longitudinal fasciculus, sagittal stratum and the superior fronto-occipital fasciculus (43).

The white matter (WM) of the human brain has been attracting much attention of neuroscientists as an important area affected by various neurodegenerative diseases. When exploring the role of the corpus callosum (CC), basal ganglia and cerebellum in a psychiatric disorder, it is relevant to examine the

microstructural characteristics besides the macroanatomical features.

The CC is the main commissural white matter bundle interconnecting the two cerebral hemispheres in a dynamic and flexible interaction (13). Dramshdal et al (2012) found that the isthmus/splenium part of the CC in the ADHD group showed reduced FA values compared to the control group (13). We found significantly higher MD values in the ADHD group relative to the control corpus callosum (BCC, GCC) at the left side. Significantly increased FA were found in ADHD patients in the corpus callosum (SCC, GCC, BCC). According to literature, reduced FA values may indicate a reduction in either size, myelination or number of axons passing through this subregion of the CC.

The basal ganglia are suggested to play the major role in the pathophysiology of ADHD so most of studies have chosen the caudate nucleus, globus pallidus/putamen and the thalamus as their regions of interest. Some workers hypothesized that children with ADHD would have abnormal diffusion properties in these areas particularly in the caudate nucleus that is the center of fronto-striatal networks (44). They found no significant group differences in either FA or MD for any of the ROIs. We found significantly higher MD, FA, RD and AD values in the ADHD group relative to the controls for the substantia nigra, amiygdala, caudate, thalamus, hippocampus and red nucleus.

The cerebellum is an important structure because of its structural disturbances in ADHD as well as its role in motor contro several cognitive processes and affective processes (45). Prior volumetric MRI studies have reported anatomical abnormalities in the cerebellum of children with ADHD (5, 34). MCP (middle cerebellar peduncle) is a fibre bundle composed of afferent fibres as part of the corticopontocerebellar tract connecting the sensory and motor areas of the cortex with the pons and cerebellum. Bescht et al. (2009) found decreased anisotropy for the ADHD group in the right MCP (45). Ashtari et al. (2005) found decreased FA values in the cerebellar region in children with ADHD (8). We found significantly higher MD values in the ADHD group relative to the controls, in MCP, SCP, ICP and the cerebellum. Significantly higher RD values were seen in the ADHD group relative to the controls, bilaterally in MCP, SCP and ICP. There is a link between the cerebellum and higher order functions through the corticopontocerebellar circuit via the MCP. This fiber pathway consists of a feedforward and feedback limb. The feedforward limb is composed of the corticopontine and pontocerebellar fiber projection that carries associative, paralimbic, sensory and motor information from the cerebral cortex to the pons. The feedback loop consists of the cerebellothalamic and thalamocortical pathways (8). We suggest that bilaterally increased MD and RD values at the level of the MCP, ICP and SCP can play a greater role in ADHD patients.

The two studies of adults showed decreased FA and greater MD in ADHD limited to later-maturing prefrontal white matter including the anterior cingulum (46, 47), orbitofrontal white matter (46) and anterior frontoparietal white matter pathways (47). Silk et al. (2009) also showed decreased radial diffusion in white matter of youths with ADHD, but in association with increased (not decreased) axial diffusion (14). Nagel et al. (2011) found decreased FA in frontoparietal, frontolimbic, cerebellar, corona radiata and temporooccipital white matter compared with the controls (3). In addition, ADHD was associated with lower MD in the posterior limb of the internal capsule and frontoparietal white matter and greater MD in frontolimbic white matter (3).

There are very few studies reporting DTI changes in brain structure in ADHD (8, 14, 43) by using a whole-brain voxel-based morphology (VBM) analysis technique and reported decreased FA in children with ADHD. Silk et al. (2009) used ROI analysis and found that mean FA and MD values were very similar between control and ADHD groups in each of the basal ganglia ROIs ($P>0.05$). van Evijk (2014) stated that individuals with ADHD showed decreased FA and decreased MD in several widespread, non-overlapping brain regions. In contrast, higher ADHD symptom count was consistently associated with increased FA and decreased MD in the ADHD group (43).

VBA studies, exploring the whole brain for white matter abnormalities, have become increasingly popular during recent years (11, 43). Ashtari et al. (2005) compared children with ADHD-C and well-matched healthy controls aged 7–11 years. They studied FA throughout the whole brain using voxel-wise analysis approach and reported decreased FA in children with ADHD in the right premotor, right striatal and left parieto-occipital areas as well as the right cerebral peduncle, left middle cerebellar peduncle and left cerebellum (anterior lobe) (8).

Another VBA study found three distinct clusters of increased FA in ADHD patients within right parietal–occipital regions, left inferior frontal cortex/striatum and left inferior temporal regions. For most clusters, significant increases in axial diffusivity were found, but also decreases in radial diffusivity. There were no MD differences between ADHD patients and control participants (14). The findings indicate that the greater FA found in ADHD might result from less neuronal branching in the investigated WM pathways (11). Kondrad et al (2010) found that elevated MD in patients in the left superior longitudinal fasciculus as well as bilaterally in orbitofrontal WM, including the inferior fronto-occipital fasciculus and uncinate fasciculus, extending into the anterior thalamic radiation (46). Nagel et al (2011) reported decreased FA in frontoparietal, frontolimbic and cerebellar structures as well as in the corona radiata and temporooccipital WM, as compared with controls (3). Additionally, lower MD was found in the posterior internal capsule and frontoparietal WM and greater MD in the frontolimbic WM. Although FA/MD differences were due to a combination of differences in both axial and radial diffusivity between groups, differences were most apparent in the frontolimbic WM in which the ADHD group showed increased radial diffusivity. These results indicate that especially the later maturing frontolimbic pathways were abnormal in children with ADHD, seemingly due to decreased or delayed myelination of these areas (3).

In very young children with ADHD, increased radial diffusivity was shown in frontolimbic areas so suggesting delayed myelin development in these regions (3). Decreased FA in patients might either be caused by axonal damage or can be found in areas with decreased or delayed myelination. Elevated FA represents greater directionality of diffusion and is thus associated with less neuronal branching in patients (43). For instance, a reduction in FA could be due to a reduction in axial diffusivity or an increase in radial diffusivity or a combination of both. While decreases in axial diffusivity are thought to be indicative of axonal damage or degeneration, increases in radial diffusivity with minimal changes in axial diffusivity are thought to result from increased freedom of cross-fibre diffusion and thus are likely to represent decreased myelination (10, 12). Increased mean diffusivity is related to increased volume of the extracellular space or with decreased barriers to diffusion in white matter; thus it is often a consequence of neuroinflammation or edema (48, 49).

In a quantitative meta-analysıs, van Ewijk et al. (2012) identified five clusters as being reported across studies, located in the right anterior corona radiata (likely containing fibres from the superior longitudinal fasciculus), forceps minor close to the genu of the corpus callosum, right and left internal capsule and left cerebellar WM (3, 41, 50, 51).

Thıs study has some limitations: We included patients with ADHD who were receiving treatment. However, we found no evidence that treatment status affected the findings. There were no differences in fractional anisotropy or mean diffusivity in participants on and off pharmacotherapy. Another limitation is the small sample size: 17 ADHD subjects and 10 controls.

We used MriStudios softwares for ABA. MriStudio is a recent analysis software developed specifically for DTI data for whole-brain volume. We found that increased MD, AD and RD values in brain structures and some is bilaterally or not. We found also increased lateral ventricle volume bilaterally. There is no result about the lateral ventricular volume differences for ADHD in the literature. Our results showed that, compared with healthy controls, patients with ADHD showed increased fractional anisotropy in bilateral regions of the SCC, as well as the right PLIC, SCR, ACR, and decreased in the bilateral region of the subgenual ACC. Patients also had increased bilateral MD in the caudate, substantia nigra, amigdala, hippocampus and cerebellum compared with the controls. Patients also had increased bilateral RD in the entorhinal area, MCP, caudate, substantia nigra, thalamus and hippocampus compared with the controls. In addition, patients had decreased bilateral AD in the red nucleus compared with the controls. We found a significantly decreased FA value in the right and left subgenual anterior cingulate gyrus.

Conclusion

MD and RD can provide us with a useful parameters to investigate the integrity of white matter tracts at the microstructural level and shed new light on the pathophysiology of brain WM in ADHD patients. The observation of a significant elevation in axial and mean as well as radial diffusivities in children with ADHD points out the important role of WM in the pathogenesis of this disorder. The differences in WM between cases and controls also points to the possibility of underlying myelination changes. Mean and radial diffusivity may provide specific insights into the neurobiological nature of axonal abnormalities and so provide more accurate interpretation of DTI findings.

Abbreviations

ABA	Atlas based analysis
ACC	Accuracy rate
ACR	Anterior corona radiata
AD	Axial diffusivity
ADHD	Attention deficit/hyperactivity disorder
AG_R	Angular gyrus right,
AIR	Automated image registration,
Amyg	Amygdala
AnteriorCom_L	Anterior commissure left
Caud_R	Caudate nucleus
CGH_L	Cingulum (hippocampus) left
CP	Cerebral peduncle
CP_R	Cerebral peduncle right
CST_L	Corticospinal tract left
CST_R	Corticospinal tract right
DTI	Diffusion tensor imaging
EC_L	External capsule left
ENT	Entorhinal area
FA	Fractional anisotropy
Fx	Fornix (column and body of fornix)
Fx/ST	Fornix (cres) / Stria terminalis (can not be resolved with current resolution)
GP_L	Globus pallidus left
Hippo	Hippocampus
Hippo_R	Hippocampus right
ICP_L	Inferior cerebellar peduncle left
Ins	Insular
LenticularFasc	Lenticular fasciculus
LenticularFasc_R	Lenticular fasciclus right
IFG_triangularis	Inferior frontal gyrus pars triangularis
left subcallosal_ACC	Subcallosal anterior cingulate gyrus
LDDMM	Large deformation diffeomorphic metric mapping
LFOG_L	Lateral fronto-orbital gyrus left
LV_atrium_R	Lateral ventricle_atrium right
LV_body_L	Lateral ventricle_body left
LV_body_R	Lateral ventricle_body right
LV_body	Lateral ventricle_body
LV_atrium_L	Lateral ventricle_atrium
LV_occipital_L	Lateral ventricle_occipital
LV_frontal_R	Lateral ventricle_frontal
Medulla_L	Medulla left
MD	Mean diffusivity
MFG_DPFC_R	Middle frontal gyrus (dorsal prefrontal cortex) right
Midbrain	Midbrain
MCP	Middle cerebellar peduncle

ML	Medial lemniscus
ML_R	Medial lemniscus right
MOG_L	Middle occipital gyrus left
MTG	Middle temporal gyrus
MTGpole	Pole of Middle temporal gyrus
MTG_R	Middle temporal gyrus right
Mynert	Nucleus innominata of Mynert
NPV	Negative predictive value
PCR_L	Posterior corona radiata left
PCT	Pontine crossing tract (a part of MCP)
OlfactoryRadiation	Olfactory radiation
PCR	Posterior corona radiata
PCT_L	Pontine crossing tract (a part of MCP) left
PCT_R	Pontine crossing tract (a part of MCP) right
PHG	Parahippocampal gyrus
PLIC	Posterior limb of internal capsule
PLIC_L	Posterior limb of internal capsule left
PPV	Positive predictive value
PSIG_R	Posterior inferior temporal gyrus right
Pons	Pons
PSMG_L	Posterior middle temporal gyrus left
PSMG_R	Posterior middle temporal gyrus right
PSTG_R	Posterior superior temporal gyrus right
PTR	Posterior thalamic radiation (include optic radiation)
Put	Putamen
PSTG	Posterior superior temporal gyrus
RD	Radial diffusivity
RedNc	Red Nucleus
RG	Gyrus rectus
RLIC	Retrolenticular part of internal capsule
RLIC_L	Retrolenticular part of internal capsule left
RLIC_R	Retrolenticular part of internal capsule right,
rostral_ACC	Rostral anterior cingulate gyrus
SCC_L	Splenium of corpus callosum left
SCC_R	Splenium of corpus callosum right
SCP	Superior cerebellar peduncle
SCP_R	Superior cerebellar peduncle right
SEN	Sensitivity
SFG	Superior frontal gyrus (posterior segment
SFG_pole	Superior frontal gyrus (frontal pole)
SLF	Superior longitudinal fasciculus
SFO	Superior fronto-occipital fasciculus (could be a part of anterior internal capsule)
Snigra	Substancia nigra
Snigra_L	Substancia nigra left
SPE	Specificity
STG	Superior temporal gyrus
STGpole	Pole of Superior temporal gyrus
subgenual_ACC	Subgenual anterior cingulate gyrus
TAP	Tapatum
Thal	Thalamus
UNC	Uncinate fasciculus
VBM	Voxel-based morphometry
WM	White matter

Acknowledgments

The authors thank Hale Acer for her skilful technical assistance. We also thank Dr. Mohamed Lehar for critical reading of the manuscript and language editing. This work is funded by the Scientific and Technological Research Council of Turkey (TUBITAK) 1002 Project (114S149).

Conflict of interest statement

All authors disclose any actual or potential conflict of interest.

Ethical approval

All experimental procedures were approved by the Erciyes Universty Ethics Board.

References

1. Tajima-Pozo K, Ruiz-Manrique G, Yus M, Arrazola J, Montañes-Rada F. Correlation between amygdala volume and impulsivity in adults with attention-deficit hyperactivity disorder. Acta Neuropsychiatr 2015; 27(6): 362-7.
2. Carrey N, Bernier D, Emms M, Gunde E, Sparkes S, Macmaster FP, Rusak B. Smaller volumes of caudate nuclei in prepubertal children with ADHD: impact of age. J Psychiatr Res 2012; 46(8): 1066-72.
3. Nagel BJ, Bathula D, Herting M, Schmitt C, Kroenke CD, Fair D, Nigg JT. Altered white matter microstructure in children with attention-deficit/hyperactivity disorder. J Am Acad Child Adolesc Psychiatry 2011; 50(3): 283-92.
4. Shaw P, Rabin C. New insights into attention-deficit/hyperactivity disorder using structural neuroimaging. Curr Psychiatry Rep 2009; 11(5): 393-8.
5. Mostofsky SH, Cooper KL, Kates WR, Denckla MB, Kaufmann WE. Smaller prefrontal and premotor volumes in boys with attention-deficit/hyperactivity disorder. Biol Psychiatry 2002; 52(8): 785-94.
6. Filipek PA, Semrud-Clikeman M, Steingard RJ, Renshaw PF, Kennedy DN, Biederman J. Volumetric MRI analysis comparing subjects having attention-deficit hyperactivity disorder with normal controls. Neurology 1997; 48(3): 589-601.
7. Sasayama D, Hayashida A, Yamasue H, Harada Y, Kaneko T, Kasai K, Washizuka S, Amano N. Neuroanatomical correlates of attention-deficit-hyperactivity disorder accounting for comorbid oppositional defiant disorder and conduct disorder. Psychiatry Clin Neurosci 2010; 64(4): 394-402.
8. Ashtari M, Kumra S, Bhaskar SL, Clarke T, Thaden E, Cervellione KL, Rhinewine J, Kane JM, Adesman A, Milanaik R, Maytal J, Diamond A, Szeszko P, Ardekani BA. Attention-deficit/hyperactivity disorder: a preliminary diffusion tensor imaging study. Biol Psychiatry 2005; 57(5): 448-55.
9. Beaulieu C. The basis of anisotropic water diffusion in the nervous system - a technical review. NMR Biomed 2002; 15(7-8): 435-55.
10. Alexander AL, Lee JE., Lazar M., Aaron S. Field. Diffusion tensor imaging of the brain. Neurotherapeutics 2007; 4(3): 316-29.
11. van Ewijk H, Heslenfeld DJ, Zwiers MP, Buitelaar JK, Oosterlaan J. Diffusion tensor imaging in attention deficit/hyperactivity disorder: a systematic review and meta-analysis. Neurosci Biobehav

Rev 2012; 36(4): 1093-106.
12. Song SK, Sun SW, Ramsbottom MJ, Chang C, Russell J, Cross AH. Dysmyelination revealed through MRI as increased radial (but unchanged axial) diffusion of water. Neuroimage 2002; 17(3): 1429-36.
13. Dramsdahl M, Westerhausen R, Haavik J, Hugdahl K, Plessen KJ. *Adults with attention-deficit/hyperactivity disorder - a diffusion-tensor imaging study of the corpus callosum.* Psychiatry Res 2012; 201(2): 168-73.
14. Silk TJ, Vance A, Rinehart N, Bradshaw JL, Cunnington R. *White-matter abnormalities in attention deficit hyperactivity disorder: a diffusion tensor imaging study.* Hum Brain Mapp 2009; 30(9): 2757-65.
15. Faria AV, Zhang J, Oishi K, Li X, Jiang H, Akhter K, Hermoye L, Lee SK, Hoon A, Stashinko E, Miller MI, van Zijl PC, Mori S. *Atlas-based analysis of neurodevelopment from infancy to adulthood using diffusion tensor imaging and applications for automated abnormality detection.* Neuroimage 2010; 52(2): 415-28.
16. Yoshida S, Faria AV, Oishi K, Kanda T, Yamori Y, Yoshida N, Hirota H, Iwami M, Okano S, Hsu J, Li X, Jiang H, Li Y, Hayakawa K, Mori S. *Anatomical characterization of athetotic and spastic cerebral palsy using an atlas-based analysis.* J Magn Reson Imagin 2013; 38(2): 288-98.
17. Faria AV, Hoon A, Stashinko E, Li X, Jiang H, Mashayekh A, Akhter K, Hsu J, Oishi K, Zhang J, Miller MI, van Zijl PC, Mori S. *Quantitative analysis of brain pathology based on MRI and brain atlases--applications for cerebral palsy.* Neuroimage 2011; 54(3): 1854-61.
18. Jiang H, van Zijl PC, Kim J, Pearlson GD, Mori S. *DtiStudio: resource program for diffusion tensor computation and fiber bundle tracking.* Comput Methods Programs Biomed 2006; 81(2): 106-16.
19. Ceritoglu C, Tang X, Chow M, Hadjiabadi D, Shah D, Brown T, Burhanullah MH, Trinh H, Hsu JT, Ament KA, Crocetti D, Mori S, Mostofsky SH, Yantis S, Miller MI, Ratnanather JT. *Computational analysis of LDDMM for brain mapping.* Front Neurosci 2013; 7: 151.
20. Dogan MS, Gumus K, Koc G, Doganay S, Per H, Gorkem SB, Canpolat M, Bayram AK, Coskun A. *Brain diffusion tensor imaging in children with tuberous sclerosis.* Diagn Interv Imaging 2016; 97(2): 171-6.
21. Miller MI, Beg MF, Ceritoglu C, Stark C. *Increasing the power of functional maps of the medial temporal lobe by using large deformation diffeomorphic metric mapping.* Proc Natl Acad Sci U S A, 2005; 102(27): 9685-90.
22. Oishi K, Faria A, Jiang H, Li X, Akhter K, Zhang J, Hsu JT, Miller MI, van Zijl PC, Albert M, Lyketsos CG, Woods R, Toga AW, Pike GB, Rosa-Neto P, Evans A, Mazziotta J, Mori S. *Atlas-based whole brain white matter analysis using large deformation diffeomorphic metric mapping: application to normal elderly and Alzheimer's disease participants.* Neuroimage 2009; 46(2): 486-99.
23. Ennis DB, Kindlmann G. *Orthogonal tensor invariants and the analysis of diffusion tensor magnetic resonance images.* Magn Reson Med 2006; 55(1): 136-46.
24. Bilgen M. *Imaging corticospinal tract connectivity in injured rat spinal cord using manganese-enhanced MRI.* BMC Medical Imaging 2006; 6:15.
25. Bilgen M, Narayana PA. *Mohr diagram interpretation of anisotropic diffusion indices in MRI.* Magn Reson Imaging 2003; 21(5): 567-72.
26. Pierpaoli C, Basser PJ. *Toward a quantitative assessment of diffusion anisotropy.* Magn Reson Med 1996; 36(6): 893-906.
27. Winston GP. *The physical and biological basis of quantitative parameters derived from diffusion MRI.* Quant Imaging Med Surg 2012; 2(4): 254-65.
28. Bilgen M, Elshafiey I, Narayana PA. *Mohr diagram representation of anisotropic diffusion tensor in MRI.* Magn Reson Med 2002; 47(4): 823-7.
29. Bilgen M, Heddings A, Al-Hafez B, Hasan W, McIff T, Toby B, Nudo R, Brooks WM. *Microneurography of human median nerve.* J Magn Reson Imaging 2005; 21(6): 826-30.
30. Radoeva PD, Coman IL, Antshel KM, Fremont W, McCarthy CS, Kotkar A, Wang D, Shprintzen RJ, Kates WR *Atlas-based white matter analysis in individuals with velo-cardio-facial syndrome (22q11.2 deletion syndrome) and unaffected siblings.* Behav Brain Funct 2012; 8: 38.
31. Hochberg Y, Benjamini Y. *More powerful procedures for multiple significance testing.* Stat Med 1990; 9(7): 811-8.
32. Tibshirani R, Hastie T, Narasimhan B, Chu G. *Diagnosis of multiple cancer types by shrunken centroids of gene expression.* Proc Natl Acad Sci U S A 2002; 99(10): 6567-72.
33. Gregory R. Warnes, B.B., Lodewijk Bonebakker, Robert Gentleman, Wolfgang Huber Andy Liaw, Thomas Lumley, Martin Maechler, Arni Magnusson, Steffen Moeller, Marc Schwartz and Bill Venables *(2015). gplots: Various R Programming Tools for Plotting Data. R package version 2.16.0.* . 2015.
34. Castellanos FX, Giedd JN, Marsh WL, Hamburger SD, Vaituzis AC, Dickstein DP, Sarfatti SE, Vauss YC, Snell JW, Lange N, Kaysen D, Krain AL, Ritchie GF, Rajapakse JC, Rapoport JL. *Quantitative brain magnetic resonance imaging in attention-deficit hyperactivity disorder.* Arch Gen Psychiatry 1996; 53(7): 607-16.
35. Giedd JN, Castellanos FX, Casey BJ, Kozuch P, King AC, Hamburger SD, Rapoport JL. *Quantitative morphology of the corpus callosum in attention deficit hyperactivity disorder.* Am J Psychiatry 1994; 151(5): 665-9.
36. Mostofsky SH, Reiss AL, Lockhart P, Denckla MB. *Evaluation of cerebellar size in attention-deficit hyperactivity disorder.* J Child Neurol 1998; 13(9): 434-9.
37. Lopez-Larson MP, King JB, Terry J, McGlade EC, Yurgelun-Todd D,. *Reduced insular volume in attention deficit hyperactivity disorder.* Psychiatry Res 2012; 204(1): 32-9.
38. Castellanos FX, Sharp WS, Gottesman RF, Greenstein DK, Giedd JN, Rapoport JL. *Anatomic brain abnormalities in monozygotic twins discordant for attention deficit hyperactivity disorder.* Am J Psychiatry 2003; 160(9): 1693-6.
39. Garrett A, Penniman L, Epstein JN, Casey BJ, Hinshaw SP, Glover G, Tonev S, Vitolo A, Davidson M, Spicer J, Greenhill LL, Reiss AL. *Neuroanatomical abnormalities in adolescents with attention-deficit/hyperactivity disorder.* J Am Acad Child Adolesc Psychiatry 2008; 47(11): 1321-8.
40. Mataró M, Garcia-Sánchez C, Junqué C, Estévez-González A, Pujol J. *Magnetic resonance imaging measurement of the caudate nucleus in adolescents with attention-deficit hyperactivity disorder and its relationship with neuropsychological and behavioral measures.* Arch Neurol 1997; 54(8): 963-8.
41. Qiu A, Crocetti D, Adler M, Mahone EM, Denckla MB, Miller MI, Mostofsky SH. *Basal ganglia volume and shape in children*

with attention deficit hyperactivity disorder. Am J Psychiatry 2009; 166(1): 74-82.

42. Batty MJ, Liddle EB, Pitiot A, Toro R, Groom MJ, Scerif G, Liotti M, Liddle PF, Paus T, Hollis C. *Cortical gray matter in attention-deficit/hyperactivity disorder: a structural magnetic resonance imaging study.* J Am Acad Child Adolesc Psychiatry 2010; 49(3): 229-38.
43. van Ewijk H, Heslenfeld DJ, Zwiers MP, Faraone SV, Luman M, Hartman CA, Hoekstra PJ, Franke B, Buitelaar JK, Oosterlaan J. *Different mechanisms of white matter abnormalities in attention-deficit/hyperactivity disorder: a diffusion tensor imaging study.* J Am Acad Child Adolesc Psychiatry 2014; 53(7): 790-9.
44. Silk TJ, Vance A, Rinehart N, Bradshaw JL, Cunnington R. *Structural development of the basal ganglia in attention deficit hyperactivity disorder: a diffusion tensor imaging study.* Psychiatry Res 2009; 172(3): 220-5.
45. Bechtel N, Kobel M, Penner IK, Klarhöfer M, Scheffler K, Opwis K, Weber P. *Decreased fractional anisotropy in the middle cerebellar peduncle in children with epilepsy and/or attention deficit/hyperactivity disorder: a preliminary study.* Epilepsy Behav 2009; 15(3): 294-8.
46. Konrad A, Dielentheis TF, El Masri D, Bayerl M, Fehr C, Gesierich T, Vucurevic G, Stoeter P, Winterer G. *Disturbed structural connectivity is related to inattention and impulsivity in adult attention deficit hyperactivity disorder.* Eur J Neurosci 2010; 31(5): 912-9.
47. Makris N, Buka SL, Biederman J, Papadimitriou GM, Hodge SM, Valera EM, Brown AB, Bush G, Monuteaux MC, Caviness VS, Kennedy DN, Seidman LJ. *Attention and executive systems abnormalities in adults with childhood ADHD: A DT-MRI study of connections.* Cereb Cortex 2008; 18(5): 1210-20.
48. Syková E.*Diffusion properties of the brain in health and disease.* Neurochem Int 2004; 45(4): 453-66.
49. Lochner C, Fouché JP, du Plessis S, Spottiswoode B, Seedat S, Fineberg N, Chamberlain SR, Stein DJ. *Evidence for fractional anisotropy and mean diffusivity white matter abnormalities in the internal capsule and cingulum in patients with obsessive-compulsive disorder.* J Psychiatry Neurosci 2012; 37(3): 193-9.
50. Davenport ND, Karatekin C, White T, Lim OK. *Differential fractional anisotropy abnormalities in adolescents with ADHD or schizophrenia.* Psychiatry Res 2010; 181(3): 193-8.
51. Li Q, Sun J, Guo L, Zang Y, Feng Z, Huang X, Yang H, Lv Y, Huang M, Gong Q. *Increased fractional anisotropy in white matter of the right frontal region in children with attention-deficit/hyperactivity disorder: a diffusion tensor imaging study.* Neuro Endocrinol Lett 2010; 31(6): 747-53.